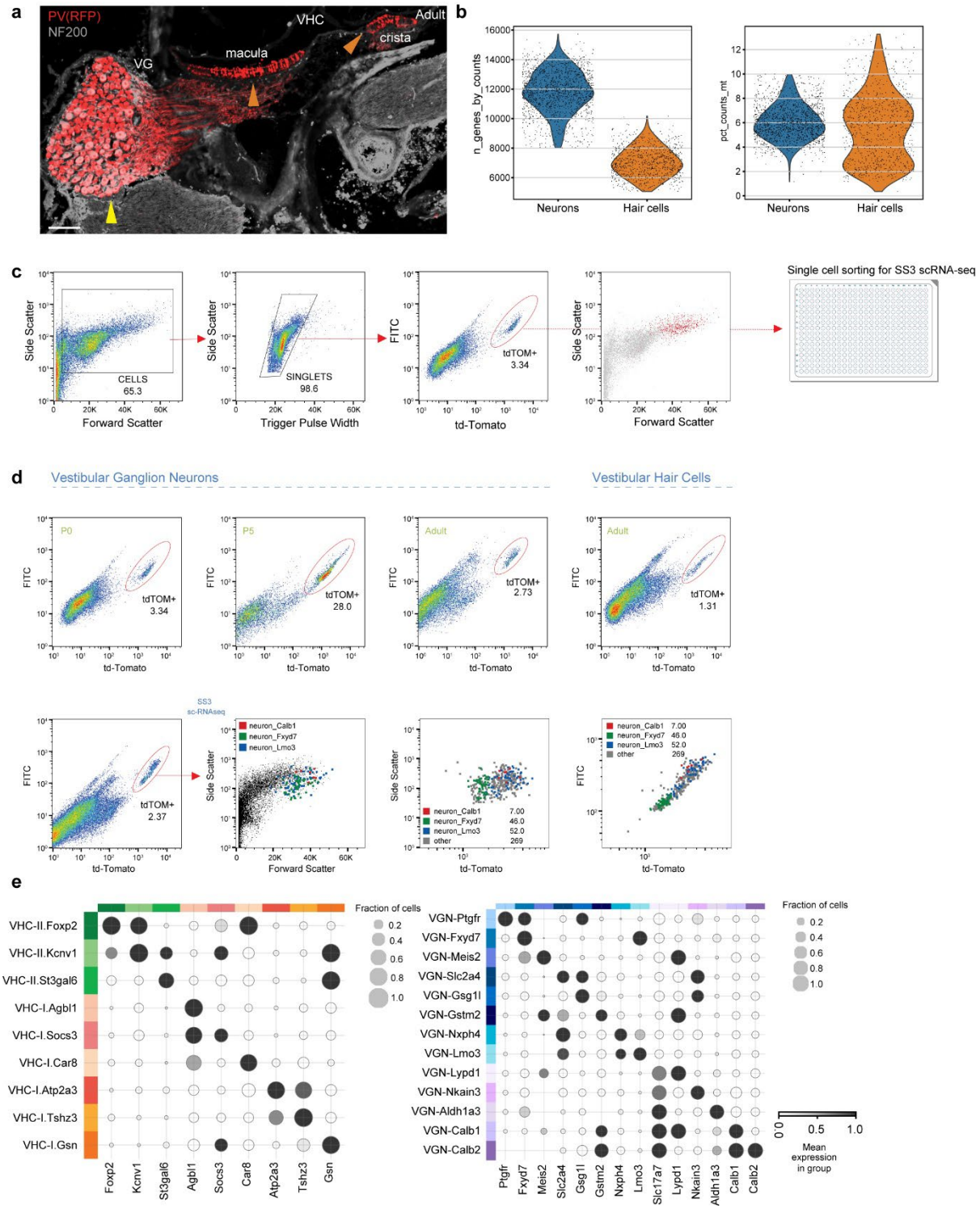

Supplementary Figure 1. FAC sorting and transcriptomic analysis of adult VGN and VHCs. a, Genetic tracing of adult VGNs (yellow arrow) and VHCs (orange arrows) with *PV^{cre};Ai14* mice. Scale bar, 100 µm **b,** Violin plots depicting genes and mtDNA detected in neurons and hair cells sorted by FACS. **c,** Schematic representation of Fluorescence activated cell sorting (FACS) of tdtomato+ neurons and hair cells. **d,** Representative FACS plots depicting gating strategy for tdtomato+ VGN and VHC capture during single cell sorting at P0, P5 and adult time points. **e,** Dot plots depict expression of pre-selected markers to define VGN and VHC subtypes.

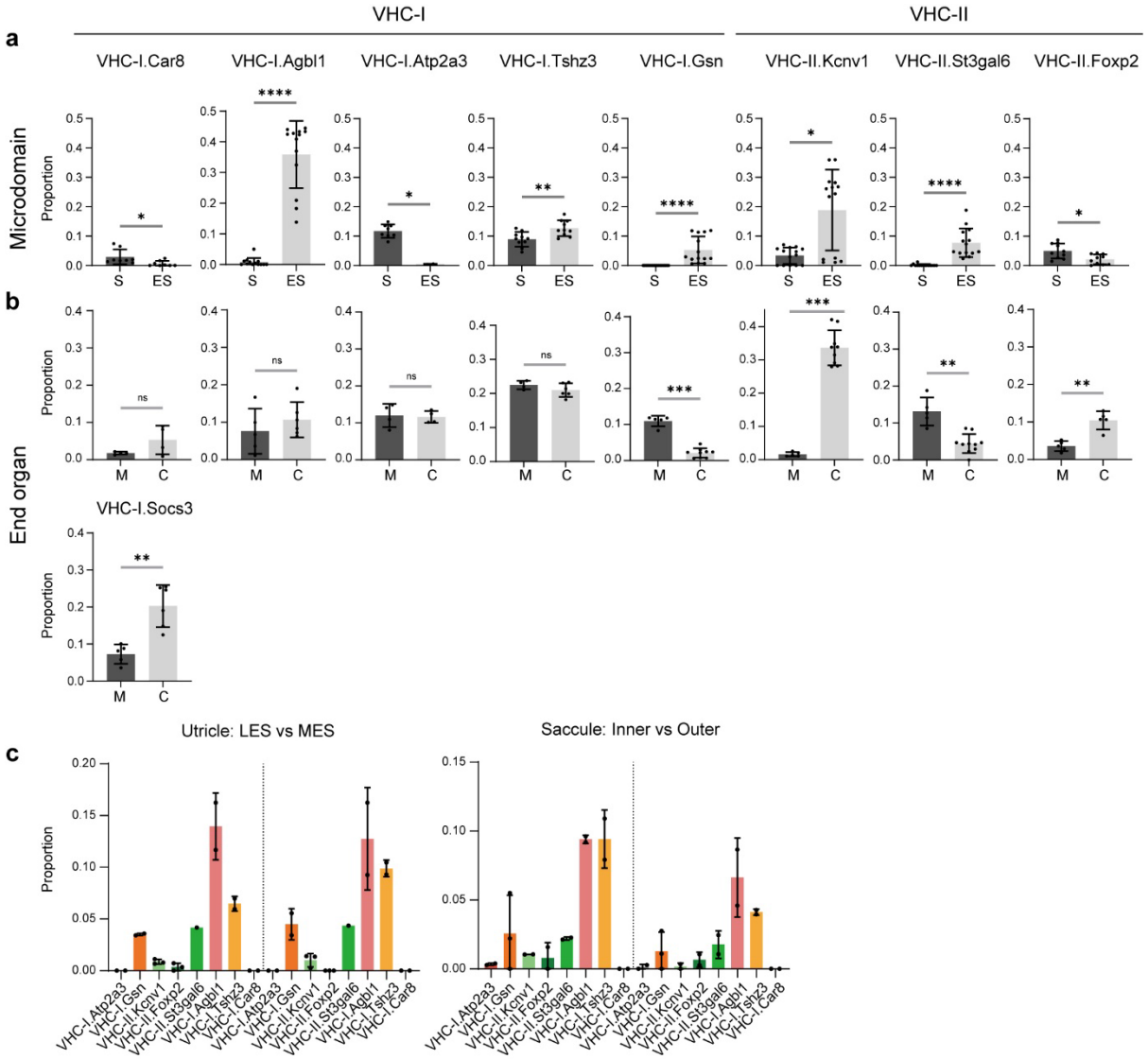

Supplementary Figure 2. Quantification of spatial distribution of VHC subtypes in sensory epithelium. a, Proportion of VHC subtypes present in Striola (S) and Extrastriola (ES) in cristae and maculae combined, Mean ± SD. **b,** Proportion of VHC subtypes in Maculae (M) and Cristae (C). **c,** Proportions of VHC subtypes distributed across domains defined by LPR (roughly estimated based on striola position and tissue morphology). Lateral Extrastriola (LES), Medial Extrastriola (MES). All data points are per end organ per animal, Mean ± SD. Mann-Whitney test, *p<0.05, **p<0.01, ***p<0.001, ****p<0.00001.

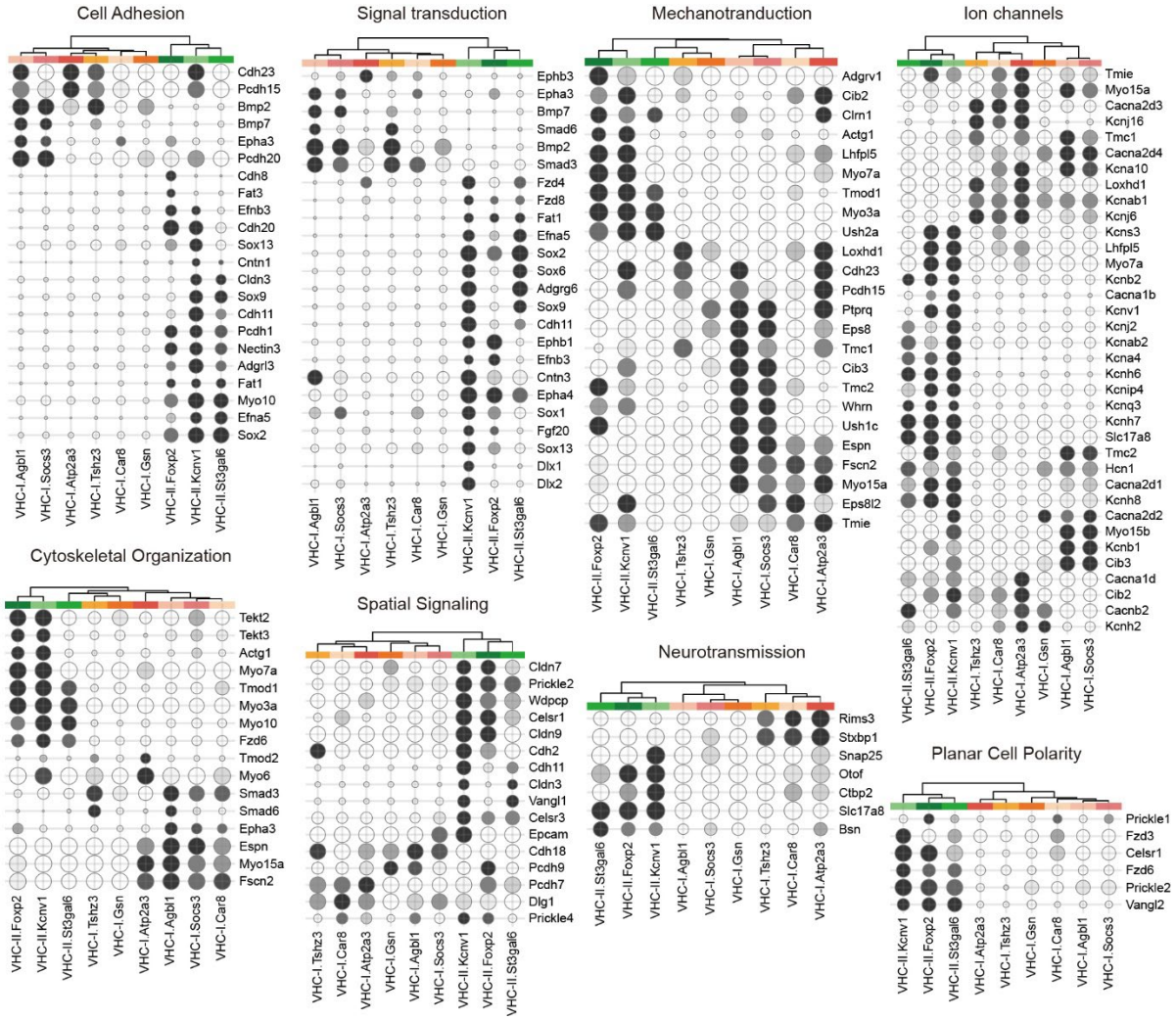

Supplementary Figure 3. Differential molecular profile of adult VHC subtypes. Dot plots of differentially expressed gene modules involved in various cellular functions, cell polarity, and spatial distribution.

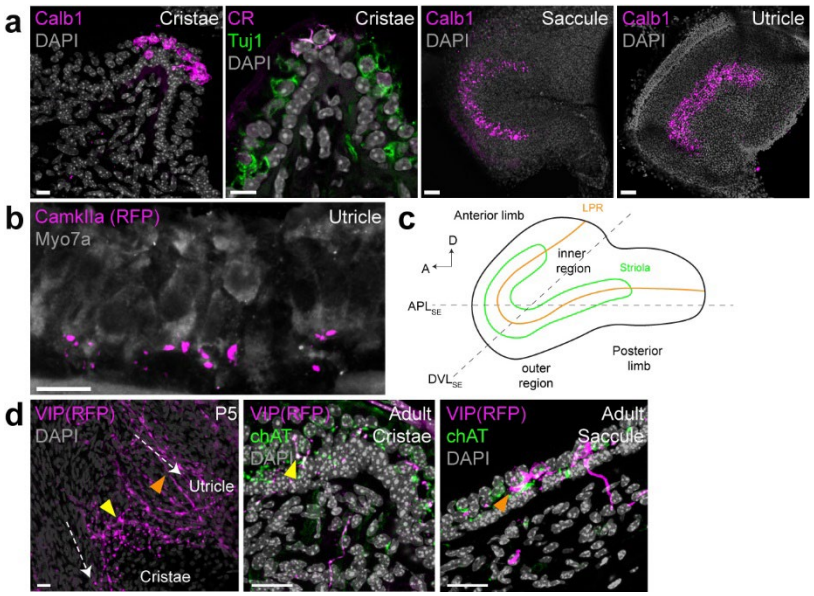

Supplementary Figure 4. Innervation patterns of VGN subtypes. a, Representative images of Calb1 and CR staining on cristae sections (Scale bar, 10 µm) and wholemounts of saccule and utricle (Scale bar, 50 µm). **b,** Genetic tracing of CamkIIa+ afferents from *CamkIIa^{creERT2};Ai14* mice labels bouton endings. Scale bar, 10 µm. **c,** Schematic representation of the morphometric features of a mouse saccular macula. APL$_{SE}$: Anterior-posterior length of the sensory epithelium; DVL$_{SE}$: Dorsal-ventral length of the saccular macula. Adapted from Desai et al. 2005[8] . **d,** Genetic tracing of VIP+ afferents from *Vip^{cre};Ai14* labels ChAT+ boutons in cristae in P5 and adult vestibular epithelium. Yellow arrows indicate *en passant* contacts and ChAT+ boutons, orange arrows indicate Vip+ afferents. Scale bar, 20 µm.

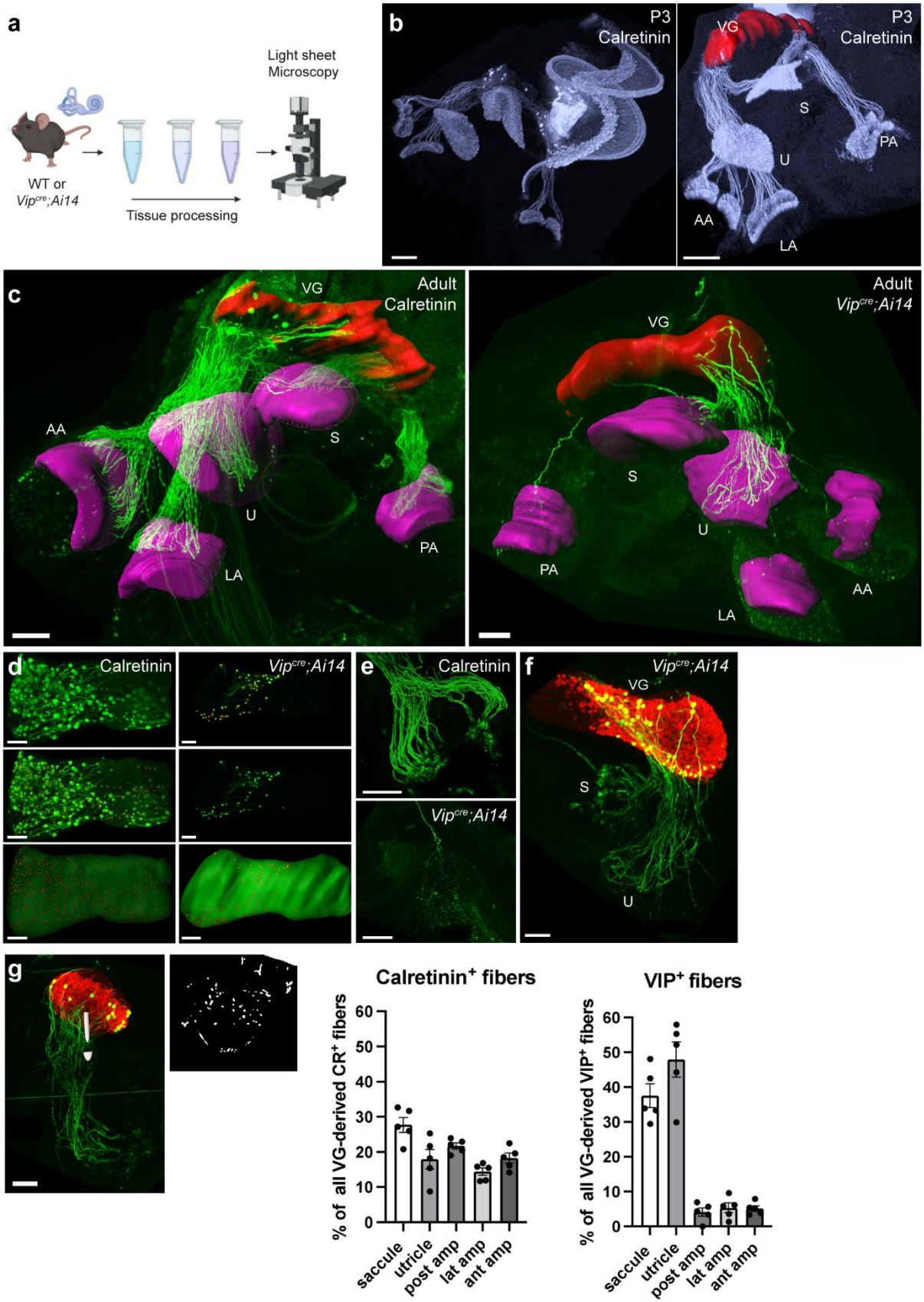

Supplementary Figure 5. Volume immuno-imaging of the inner ear. a, Workflow for high-resolution 3D visualization of the adult mouse vestibular system applying iDISCO+ volume immuno-imaging and light sheet fluorescence microscopy. **b,** 3D visualization of calretinin+

fibers and hair cells in P3 mice. Scale bar, 200 µm. **c,** Spatial distribution and characterization of nerve fibers targeting the various vestibular end organs. Overview of calretinin and VIP projections; The vestibular ganglion (red surface) and the end organs (purple surfaces). Scale bar, 150 µm. **d,** Spatial distribution of calretinin and VIP expressing neuronal populations within the vestibular ganglion. The nucleus volume is represented by a semi-transparent green surface. Each red dot represents a calretinin+ or VIP+ neuron. **e,** Calyces of calretinin+ and VIP+ nerve endings targeting the cristae. 200-mm thick optical slices from high resolution light sheet scans (0.48 mm x 0.48 mm x 2 mm X/Y/Z voxel dimensions) demonstrating calyces and boutons of individual nerve endings respectively. **f,** Optical slice of VIP+ innervation of otoliths **g,** Quantitative characterization of nerve fibers targeting the various vestibular end organs. Explanation of fiber density measurements. An oblique slicer tool was applied in Imaris software to adjust 5-mm thick optical slices perpendicular to the fiber tracts in the 3D space. These optical slices were converted to 2D images on which the area of immuno-signal (cross-sections of nerve fibers) were determined within the area of the nerve tract. The area covered by immunosignal was determined in black and white 2D images in the ROIs in Image J. Scale bar, 100 µm unless otherwise mentioned.

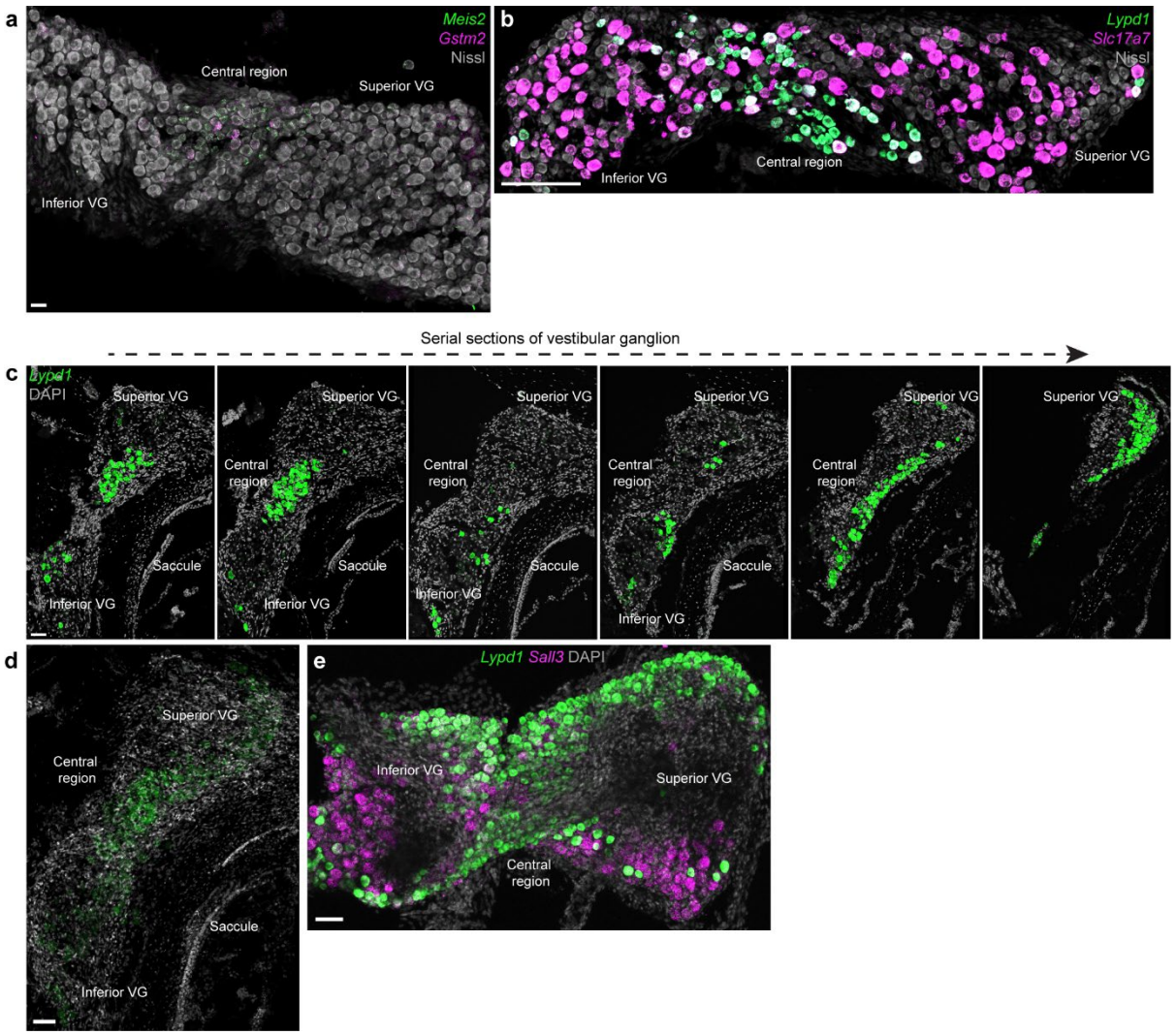

Supplementary Figure 6. Spatial distribution of Lypd1+ neurons in the Vestibular Ganglion. a,b In situ hybridization of VG with probes against *Meis2*, *Gstm2*, *Lypd1* and *Slc17a7*. **c,** Distribution of Lypd1+ VGNs in consecutive sections of vestibular ganglion in the horizontal plane starting from the cochlea and ending at the epitympanum. VGNs were labeled using probes against Lypd1 with fluorescence in situ hybridization (FISH). **d,** 3D projected view of consecutive sections using Image J. **e,** Whole mount FISH on the VG using probes against Lypd1 and Sall3 (n=3). Scale bar, 50 µm

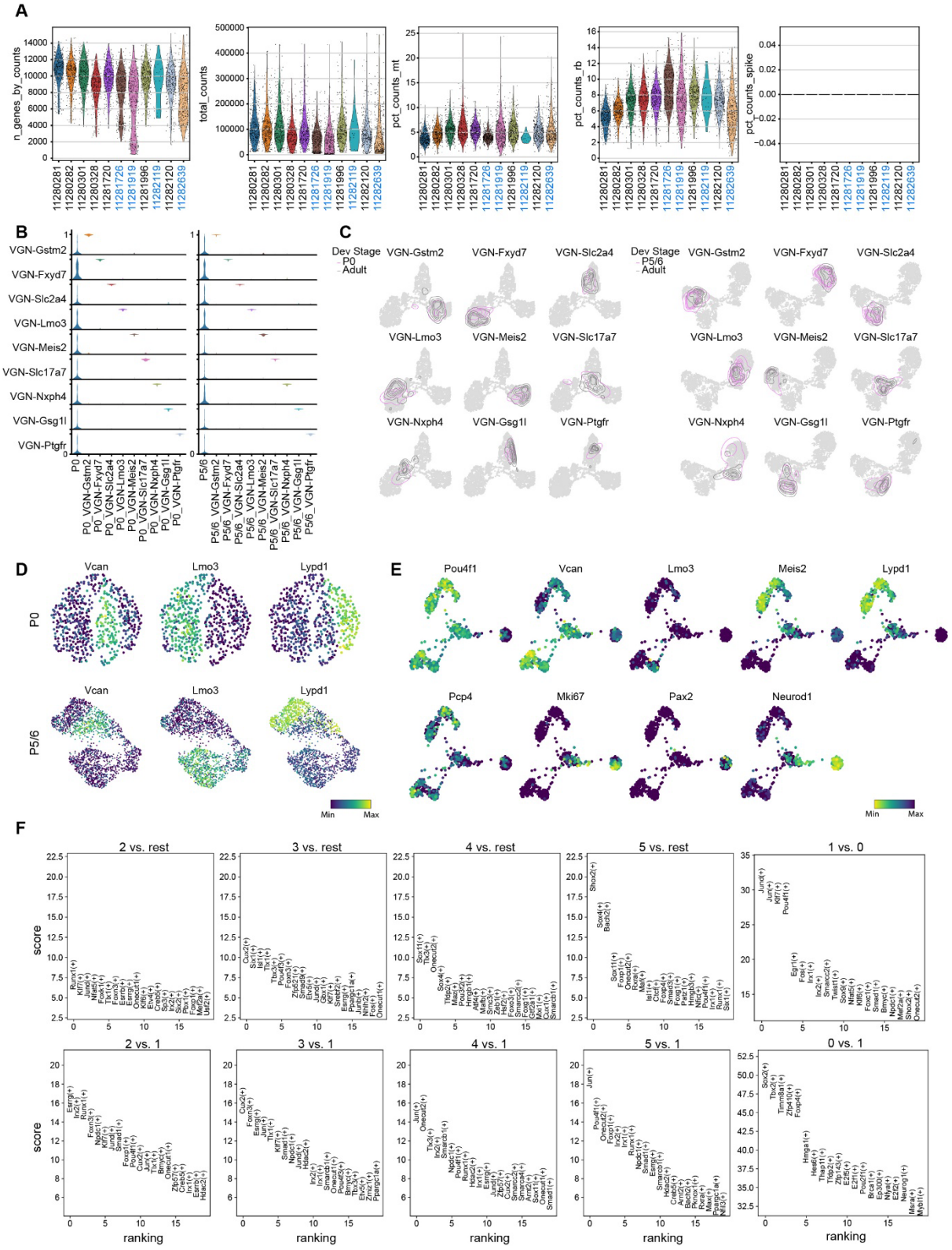

Supplementary Figure 7. Transcriptomic analysis of neonatal and embryonic VGN datasets. a, Quality control from 384 well plates following scRNAseq for P0 VGNs (in blue) and P5-6 VGNs. **b,** Violin plots showing probability mapping of subtype identity at P0 and P5/6. **c,** Kernel density plots showing probability of subtype identity mapping per VGN subtype in P0 and P5/6 datasets. **d,** Feature plots of metacluster marker genes expressed in P0 and P5/6 VGN datasets. **e,** Feature plots of key transcription factors involved in early lineage divergence.

f, Top transcription factor programs expressed in E11.5-E13.5 VGNs extracted from publicly available dataset[88].